

Phase Separation and Ripening in a Viscoelastic Gel

Tine Curk^{1,*} and Erik Luijten^{1,2,†}

¹*Department of Materials Science & Engineering,
Northwestern University, Evanston, Illinois 60208, USA*

²*Departments of Engineering Sciences & Applied Mathematics,
Chemistry and Physics & Astronomy, Northwestern University, Evanston, Illinois 60208, USA*
(Dated: March 24, 2023)

The process of phase separation in elastic solids and viscous fluids is of fundamental importance to the stability and function of soft materials. We explore the dynamics of phase separation and domain growth in a viscoelastic material such as a polymer gel. Using analytical theory and Monte Carlo simulations we report a new domain growth regime, in which the domain size increases algebraically with a ripening exponent α that depends on the viscoelastic properties of the material. For a prototypical Maxwell material, we obtain $\alpha = 1$, which is markedly different from the well-known Ostwald ripening process with $\alpha = 1/3$. We generalize our theory to systems with arbitrary power-law relaxation behavior and discuss our findings in the context of the long-term stability of materials as well as recent experimental results on phase separation in cross-linked networks and cytoskeleton.

I. INTRODUCTION

Phase separation is a universal phenomenon and a fundamental concept in physics, chemistry and materials science. Whereas its outcome is described by equilibrium thermodynamics, it is equally important to understand the dynamics of the separation process. This is particularly relevant in solid, soft and biological systems where large kinetic barriers or active processes often prevent the system from reaching its equilibrium state. Upon formation of a new phase, domains typically grow via coalescence or via surface-tension-driven dissolution and redeposition known as Ostwald ripening [1]. However, elastic effects can markedly alter the dynamics of these processes. As shown in the early days of solid-state physics, nucleation and precipitation in crystalline solids cause substantial elastic stresses, which, in turn, control the shape and growth of precipitate particles and the macroscopic mechanical properties of the material [2]. Recent experiments on droplet formation within disordered polymer networks have shown that elastic stress can either fully inhibit liquid-liquid phase separation or arrest the coarsening process [3, 4]. The latter can lead to migration of droplets in stiffness gradients, “elastic ripening” [5], which is supported by theoretical studies [6–10].

However, the situation is completely different in materials that exhibit viscoelastic relaxation or creep, which can irreversibly reduce elastic stress and thus enable further domain coarsening. Viscoelastic effects in phase separation have been extensively studied in spinodal decomposition [11], polymer solutions [12], viscoelastic fluids [13] and glass-forming melts [14–17], as well as in protein and colloidal suspensions [18, 19]. However, to the best of our knowledge phase separation of a minority phase of small molecules inside a polymer matrix has only

been studied on short time scales [3, 14], where coarsening is arrested by the elastic stress. In contrast, the long-time domain growth of nuclei or droplets is governed by the interplay between elastic forces and viscous flow. The associated coarsening laws are currently unknown. Consequently, a variety of material aging processes currently cannot be predicted.

This work was originally motivated by metal soap formation in oil paintings, an aging process believed to be driven by phase separation [20]. However, the relevance of our findings goes well beyond this topic, as it applies to various branches of materials science and is believed to play a crucial role in biological systems. Phase transitions involving biomolecular liquids have been established as fundamental drivers of intracellular organization [21, 22], and viscoelastic relaxation can enable cells to flexibly modulate mechanical properties of membrane-less organelles [23–25]. The realization that coupling between condensation and network elasticity may play a role in cellular physiology has led to renewed interest in phase separation in cells [26, 27] and in synthetic materials [3, 5].

Here, we employ analytical theory and particle-based Monte Carlo simulations to investigate the process of phase separation and surface-tension-driven coarsening within a viscoelastic medium. Focusing on a prototypical system where a minority phase forms spherical nuclei or droplets within a viscoelastic majority phase, we attain a fundamental and quantitative understanding of the coarsening process on both short and long time scales.

II. PHASE SEPARATION IN ELASTIC MEDIA

To set the stage for our investigation of viscoelasticity, we first briefly introduce elastic effects in phase separation and coarsening. We limit our analysis to the dilute regime, so that many-body elastic effects can be neglected and each droplet or precipitate can be considered an isolated spherical inclusion in an isotropic elastic

* curk@northwestern.edu

† luijten@northwestern.edu

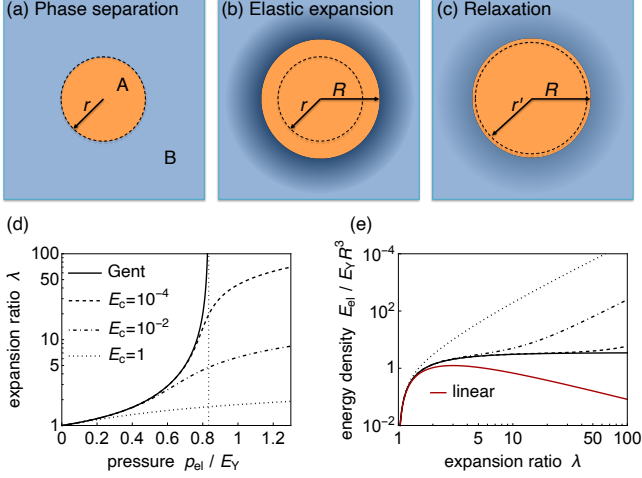


FIG. 1. Growth of a droplet in a viscoelastic medium. (a) Schematic of a minority phase A (orange) in an elastic majority phase B (blue), with r the unstressed cavity size. (b) Growth of the droplet to size $R = \lambda r$ causes elastic stresses in phase B (indicated by a darker shade of blue). (c) Viscoelastic relaxation expands the cavity to size r' , thus reducing the stress and enabling further growth of phase A. (d) Droplet size dependence on pressure for a Gent material [Eq. (1)] (solid line) and for a material with additional non-linear elasticity proportional to E_c (dashed, dot-dashed and dotted lines). The thin dotted vertical line indicates the elastic cavitation pressure $p_c = 5E_Y/6$. (e) Elastic energy density corresponding to examples in (d) and comparison with the linear elastic case (solid red line) [28].

medium (Fig. 1a). The assumption of spherical symmetry makes this problem analytically tractable. The initial cavity size r_0 is determined by the pore size in the material or the crosslink distance. For example, $r_0^3 \sim k_B T / E_Y$ for a flexible gel with Young's modulus E_Y [29], with T the absolute temperature and k_B the Boltzmann constant. An inclusion of size R growing beyond the cavity size will produce an elastic stress whose radial component at the cavity interface σ is balanced by the excess pressure within the inclusion, $p_{el} = \sigma$. (Fig. 1b). Viscoelastic relaxation can increase the cavity size, enabling further growth of the inclusion (Fig. 1c).

To describe the elastic expansion of the cavity we use the Gent model for the elastic pressure of a spherical inclusion in a rubber-like nonlinear solid [30, 31], a good approximation for cross-linked networks [3, 5, 32, 33],

$$p_{el}^{\text{Gent}}(\lambda) = \frac{E_Y}{6} \left(5 - \frac{4}{\lambda} - \frac{1}{\lambda^4} \right), \quad (1)$$

with $\lambda \equiv R/r$ the expansion ratio and r the radius of the unstressed cavity (Fig. 1). At pressures exceeding the cavitation pressure $p_c = 5E_Y/6$, elastic forces are unable to contain the inclusion and its size R increases without bounds (Fig. 1d). However, it is known that additional strain-stiffening effects can limit the size at very high λ [3, 5, 32, 33]. We account for this through

an additional term $p_{el}^{\text{lim}} = E_c E_Y (\lambda - 1)^2$, with dimensionless prefactor $E_c > 0$, that limits the expansion ratio to $\lambda_c \sim E_c^{-0.5}$ [34]. We refer to this as the extended Gent model and note that a different strain-stiffening description such as the Mooney–Rivlin model [6] or the Gent model with a set maximum strain [8], would not affect our observations. On the other hand, at small deformations ($\lambda \sim 1$) Eq. (1) reduces to $p_e = \frac{4}{3} E_Y (\lambda - 1)$, which corresponds to a standard result of linear elasticity, $p_{el} = 2E_Y (\lambda - 1) / (1 + \nu)$ [28] with Poisson ratio $\nu = 1/2$. Thus, at small deformations our findings apply to any isotropic, linear elastic material.

We note that when the size of inclusions is allowed to equilibrate through the exchange of mass via an evaporation–condensation process, the equilibrium size R can be calculated using classical nucleation theory augmented with an elastic energy term $E_{el}(\lambda)$. For a spherically symmetric system, this elastic energy equals the reversible pressure work performed by expanding the cavity from its unstressed radius r to $R = \lambda r$, $E_{el}(\lambda) = 4\pi \int_r^R r'^2 p_{el}(r'/r) dr'$. For the Gent model, the full analytical expression is provided in the Methods section [Eq. (18)]. Surface tension favors large R , while elastic pressure favors small R . Competition between surface tension and elastic stress results in a well-defined equilibrium size R [3, 5].

III. SIMULATIONS OF VISCOELASTIC RIPENING

Having described the (reversible) elastic response we emphasize that understanding the phase separation process requires a model of irreversible deformations. The simplest description of a material that is elastic on short time scales but can flow on long time scales is a Maxwell material, which is characterized by a single relaxation time τ_r . For example, supramolecular networks [13] and vitrimers [35, 36], but also covalently cross-linked polymers [37], exhibit Maxwell-type viscoelastic relaxation on sufficiently long time scales. Moreover, both crystalline and amorphous materials are generally subject to diffusion creep that follows a single time scale relaxation process. In contrast, biopolymer networks [38], protein condensates [24] and glassy materials [39] exhibit aging and relaxation over multiple time scales and are instead described by a Maxwell glass model. For example, the strain ε of cytoskeleton under stress σ increases as a power law, $\varepsilon \sim \sigma t^a$, with exponent $a \approx 0.5$ found both theoretically [40] and experimentally [41].

Coarsening processes are usually modeled using continuum mean-field theories [1], which very accurately predict growth laws in the large-domain and the long-time limits. We will develop such a theory in the next section. Modeling of small clusters on short time scales, however, requires a more detailed model that is able to accurately capture the interplay between nucleation, phase separation and viscoelastic relaxation. To this end, we

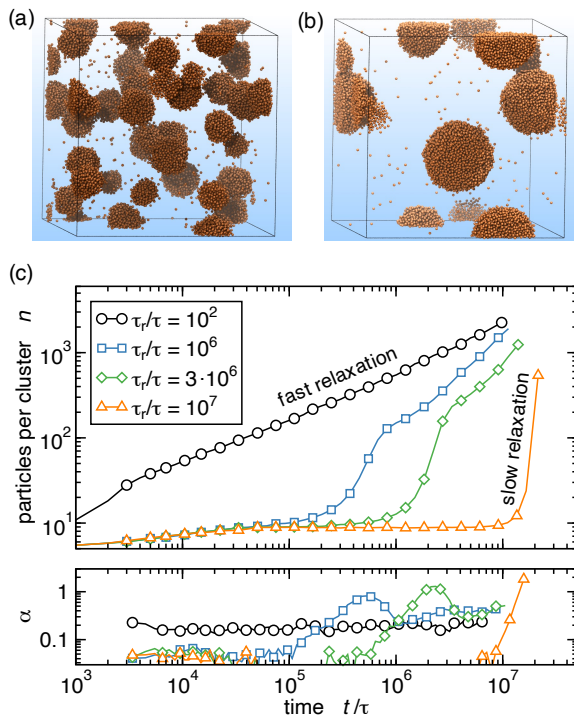


FIG. 2. Growth of condensates in a viscoelastic medium with relaxation time τ_r as determined by Monte Carlo simulations. (a,b) Snapshots at times $t = 8 \cdot 10^5 \tau$ (a) and $t = 10^7 \tau$ (b) for $\tau_r = 10^6 \tau$. Individual spherical particles with diameter d_{LJ} are shown as orange spheres and the box outline indicates periodic boundaries. (c) Top panel: Growth in the average number of particles per cluster n for various τ_r . Bottom panel: Ripening exponent α [Eq. (4)], which equals $1/3$ of the slope in the top panel, since $n \sim \bar{R}^3$. Elastic parameters: $E_Y = k_B T/d_{LJ}^3$ and $E_c = 1$.

first employ a Lennard-Jones (LJ) fluid as a prototypical particle-based model and couple it to a viscoelastic background medium with embedded spherical cavities. The configuration of this system is evolved using single-particle Monte Carlo displacement moves, modeling diffusive dynamics of individual particles. Nucleation and growth of liquid droplets within cavities causes stress and increases elastic energy. This modifies the rate at which individual particles are added to or removed from a droplet, which is accounted for through the Monte Carlo acceptance probabilities. In addition, the elastic stress leads to irreversible expansion of the cavities depending on the viscoelastic properties of the medium (see *Methods*).

The viscoelastic medium is described by the upper-convected Maxwell model [42]. In the small stress limit, this model reduces to the Maxwell model (see Supporting Information) and we use it to enable analytical predictions. For the ripening process considered, large stress can only occur when the clusters are small (stress scales as $\sigma \sim 1/R$, see Eq. (8) below), in which case the Maxwell model yields an upper bound for the coarsening rate.

Thus, we employ the Maxwell model and note that this approximation does not affect the prediction of the coarsening exponents, which are defined in the large- R limit.

For a Maxwell material at constant strain, the elastic stress σ decays exponentially, $\partial\sigma/\partial t = -\sigma/\tau_r$, on a time scale $\tau_r = \eta/E_Y$, with η the material viscosity. To avoid artifacts due to non-linear elasticity, we use a generalized form based on the reduction of the elastic energy E_{el} ,

$$\left(\frac{\partial E_{el}}{\partial t}\right)_R = -2\frac{E_{el}}{\tau_r}, \quad (2)$$

which in the linear elasticity regime corresponds exactly to the Maxwell model. Note that $E_{el} = E_{el}(R, r)$ is a state function and its time dependence arises solely through variation of the dynamical variables R and r . Factorization E_{el} [Eqs. (21) and (22) in *Methods*] and insertion into Eq. (2) leads to the expansion rate

$$\frac{dr}{dt} = \frac{2r}{\tau_r} \left[\left(\frac{\partial \ln[E_{el}/(E_Y r^3)]}{\partial \ln \lambda} \right)_R - 3 \right]^{-1}. \quad (3)$$

The Maxwell model is valid for small strain rates, $dr/dt \ll r/\tau_r$. Large strain rates require the upper-convected Maxwell model, which leads to additional shear thickening [42], but becomes analytically intractable and has not been generalized to nonlinear elasticity. For the ripening process considered, large strain rates can only occur when the clusters are small (since stress scales as $\sigma \sim 1/R$, cf. Eq.(8) below), in which case the Maxwell model yields an upper bound for the coarsening rate. Thus, we employ the Maxwell model and note that this approximation does not affect the prediction of the coarsening exponents, which are defined in the large- R limit.

The interplay of condensation and viscoelastic relaxation leads to specific dynamics of domain coarsening and cluster growth (Fig. 2), which we characterize via the growth exponent,

$$\alpha = \frac{d \log(\bar{R})}{d \log(t)}, \quad (4)$$

with \bar{R} the mean cluster radius. Under sufficiently fast relaxation ($\tau_r \rightarrow 0$), elasticity is irrelevant and the domain growth is expected to be determined by Ostwald ripening with a power-law exponent $\alpha = 1/3$ in the large-domain limit [1, 43]. In our particle-based simulations we find $\alpha \approx 0.23$ (Fig. 2c, bottom panel). This underestimation is a finite-size effect originating from the surface diffusion of individual particles [44]. However, if the viscoelastic medium relaxes more slowly, markedly different behavior results. On short time scales, $t \ll \tau_r$, the growth is limited and the evolution of cluster size is determined by elasticity [3, 5], whereas on intermediate time scales, $t \sim \tau_r$, viscoelastic relaxation enables expansion of cavities and continued domain growth. Surprisingly, we discover that in this *viscoelastic ripening* regime the exponent exceeds the Ostwald value, $\alpha > 1/3$. Since the

simulations are restricted to relatively small systems and limited time scales, we further explore the nature of this new regime, which is controlled by viscoelastic relaxation, by means of perturbation theory.

IV. VISCOELASTIC RIPENING THEORY

A. Extension of Landau–Slyozov–Wagner theory

The Landau–Slyozov–Wagner (LSW) theory of Ostwald ripening [1, 45] predicts that the average radius \bar{R} of a spherical domains grows as

$$\frac{d\bar{R}}{dt} = C c^{\text{sat}} \frac{\gamma}{\bar{R}^2}, \quad (5)$$

where c^{sat} is the monomer concentration in phase B, γ the surface tension and the prefactor $C = 8D/(27c_A^2 k_B T)$, with D the diffusion coefficient and c_A the monomer number density in the condensed phase A. The resulting power law-growth $\bar{R} \sim t^{1/3}$, is accompanied by a scale-free size distribution $h(R/\bar{R})$ [1, 43, 45].

Elastic effects alter this coarsening process in two ways. Firstly, they change the phase equilibrium between the condensed phase (A) and the viscoelastic phase (B), which is captured by an elasticity-dependent c^{sat} [5]. Assuming that the monomers in phase B are dilute and can be described by the ideal chemical potential, we find

$$c^{\text{sat}}(p_{\text{el}}) = c_0^{\text{sat}} e^{p_{\text{el}}/(c_A k_B T)}, \quad (6)$$

with the elasticity-free reference value $c_0^{\text{sat}} = c^{\text{sat}}(p_{\text{el}} \rightarrow 0)$. Secondly, the elastic energy alters the coarsening kinetics. We account for this effect using a first-order perturbation expansion of the LSW theory (see Methods section), leading to the coarsening rate

$$\frac{d\bar{R}}{dt} = C c^{\text{sat}}(p_{\text{el}}) \left[\frac{\gamma}{\bar{R}^2} - \frac{1}{4\pi} \frac{\partial [E_{\text{el}}(\bar{R}, \bar{r})/\bar{R}^3]}{\partial \bar{R}} \right]. \quad (7)$$

The elastic pressure p_{el} , the average domain radius \bar{R} and the mean cavity radius \bar{r} are all time dependent, while the prefactor C is determined by the diffusion constant D and the density of the condensed phase c_A [1]. We assume the limit in which the condensed phase A is incompressible relative to the surrounding viscoelastic phase B, and thus both c_A and C are considered constant. The surface tension γ is positive, while the elastic term in Eq. (7) can be either positive or negative depending on the elastic energy density, and thus can either accelerate or inhibit the coarsening process (cf. Fig. 1e). For example, the extended Gent model leads to growth in \bar{R} until the elastic term balances the surface tension term, at which point the growth is arrested. Prior to this arrest, \bar{R} exponentially approaches its equilibrium value, as was predicted and experimentally verified in glass-forming melts [15]. Moreover, Eq. (7) predicts that the equilibrium droplet size decreases when the elastic modulus is increased, as

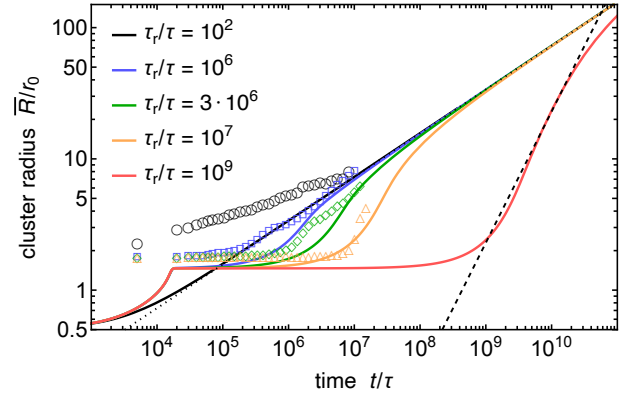


FIG. 3. Theoretical prediction for cluster growth obtained by numerical integration of Eqs. (2) and (7) (solid lines), with corresponding MC simulation results for different relaxation times, $\tau_r/\tau = 10^2$ (circles), $\tau_r/\tau = 10^6$ (squares), $\tau_r/\tau = 3 \cdot 10^6$ (diamonds) and $\tau_r/\tau = 10^7$ (triangles). The dotted black line shows the LSW theory prediction, Eq. (5), and the dashed line is the small deformation approximation to viscoelastic ripening, Eq. (9). Initial cavity diameter $r_0 = d_{LJ}$ and $E_Y = k_B T/r_0^3$.

was observed in crosslinked gels [3, 5]. In the absence of elasticity, $E_{\text{el}} = 0$, Eq. (7) reduces to the LSW theory, Eq. (5).

High droplet concentrations would induce additional interactions between droplets due to elastic distortion of the material, affecting the above predictions. However, departure from the nondilute conditions does not affect the ripening exponent in the LSW theory but only requires a rescaling of the prefactor [1]. Since elastic deformations are governed by the same algebraic profiles as the density profiles in the LSW theory, we argue that elastic interactions between droplets also will not affect the ripening exponent.

To model viscoelastic relaxation, we couple the growth of the cavity [Eq. (7)] with that of the inclusion [Eq. (3)] and integrate the two equations numerically, obtaining a prediction for domain growth (Fig. 3). Strikingly, our extension of LSW theory qualitatively captures the observations of Sec. III. In particular, we note that the perturbative solution confirms the existence of the intermediate viscoelastic ripening regime where the growth exponent, $\alpha \sim 1$, exceeds that of Ostwald ripening ($\alpha \sim 1/3$).

To directly compare the theory to the results of Fig. 2, we determine the prefactor C [Eq. (7)] from the MC simulation conditions (see Methods section). Given the first-order nature of the theory, the semi-quantitative agreement with the MC data is quite remarkable (Fig. 3). Moreover, deviations at small \bar{R} are to be expected, since LSW theory is only valid in the large-domain limit. Conversely, we note that the simulation results for the longest times exhibit quantitative agreement with the theoretical predictions. Lastly, we note that the theory illustrates how viscoelastic effects can change the predicted domain size by orders of magnitude compared to the standard

Ostwald ripening prediction.

B. Analytical theory

Whereas the perturbative solution resolves the cluster growth process across all time scales, an analytical theory would describe the viscoelastic ripening regime without the need for a numerical solution. Here we derive such a theory by assuming a small expansion ratio, $\lambda \approx 1$. In this limit, the elastic term in Eq. (7) simplifies to $\frac{1}{4\pi\bar{R}^2} \frac{\partial E_{el}(\bar{R}, \bar{r})}{\partial \bar{R}}$, which we recognize as the radial stress at the cavity wall σ . Under elastic arrest, $d\bar{R}/dt \approx 0$, the stress is thus determined solely by the surface tension,

$$\sigma \approx \gamma/\bar{R}. \quad (8)$$

We note that this approximation did not require linear elasticity assumptions. The same relation can be obtained by employing classical nucleation theory and assuming quasi-equilibrium conditions for a system of spherical clusters at constant total volume (see Sec. VI C). Combining Eq. (2), which reduces to $d\bar{r}/dt = (\lambda - 1)\bar{r}/\tau_r$, with Eq. (8) and the linear elastic stress, $\sigma = 2\tilde{E}_Y(\lambda - 1)$ [28], where $\tilde{E}_Y = E_Y/(1 + \nu)$, results in an analytical prediction for the growth rate,

$$\frac{d\bar{R}}{dt} = \frac{\gamma}{2\tau_r \tilde{E}_Y}. \quad (9)$$

This expression is valid for sufficiently large clusters, $R > \gamma/\tilde{E}_Y$, such that strain rates are low and Maxwell model is appropriate. For small clusters $R \leq \gamma/\tilde{E}_Y$ Eq. (9) represents an upper bound of the growth rate. Equation (9) is in excellent agreement with the numerical integration result in the viscoelastic ripening regime with exponent $\alpha = 1$ (dashed line in Fig. 3). Interestingly, the same expression is found for late-stage coarsening in spinodal decomposition of inter-percolating phases [11, 12], but the underlying mechanism is different. Whereas we consider an evaporation–condensation process at intermediate time scales, the coarsening of inter-percolating networks is a result of hydrodynamic flow on long time scales. Surprisingly, both cases lead to the same coarsening law, Eq. (9).

The extent of the viscoelastic ripening regime is limited by monomer diffusion, with a typical diffusion time scale $\tau_D = \bar{R}^2/D$, and a transition to Ostwald ripening occurs at sufficiently large cluster size R_c (Fig. 3). To determine the crossover size R_c , we equate the two growth rates, Eqs. (5) and (9),

$$R_c^2 = \frac{16c_{\text{sat}}}{27c_A^2} \frac{D\tau_r \tilde{E}_Y}{k_B T}. \quad (10)$$

Viscoelastic ripening is limited to $\bar{R} < R_c$ and will thus be prominent if $D\tau_r$ is large, with τ_r the Maxwell relaxation time. In a single-component phase, these

two factors are connected via the fluctuation–dissipation theorem. Employing the Stokes–Einstein relation and assuming a standard situation with a dense phase A, i.e., $c_A \sim r_m^{-3}$ with r_m the molecular size of individual monomers, we find $R_c < r_m$, so that viscoelastic ripening does not exist [46]. We conclude that viscoelastic ripening of precipitates or liquid droplets is expected to occur only in multicomponent materials that can simultaneously support both fast diffusion of monomers and sufficiently slow material relaxation. A typical example of such material is a hydrogel with a solvent viscosity that is orders of magnitude smaller than the material viscosity.

To quantitatively delineate the different growth regimes, we consider that the viscoelastic growth, Eq. (9), is noticeable upon doubling of the initial cluster size, which occurs on a time scale τ_{ve} ,

$$\tau_{ve} = \tau_r \frac{2\tilde{E}_Y r_0}{\gamma}, \quad (11)$$

whereas the transition to Ostwald ripening occurs at crossover time scale τ_c determined by Eqs. (9) and (10),

$$\tau_c = \tau_{ve} \frac{4}{c_A r_0} \sqrt{\frac{Dc_{\text{sat}}\tau_r \tilde{E}_Y}{27k_B T}}. \quad (12)$$

Thus, the distinct ripening regimes are characterized as: (i) initial growth and elastic arrest for $t < \tau_{ve}$; (ii) viscoelastic ripening with growth exponent $\alpha \approx 1$ for $\tau_{ve} < t < \tau_c$; and (iii) convergence to the LSW theory with $\alpha \approx 1/3$ for $t > \tau_c$.

C. Power-law material response

The accuracy of the analytical prediction shows that our approach can be generalized to any relaxation behavior with a strain rate that is a power-law function of both the stress $\sigma = p_{el}$ and time t ,

$$\frac{d\varepsilon}{dt} = A\sigma^b t^{a-1}, \quad (13)$$

with A a materials-dependent prefactor. This general form captures power-law fluids as well as a variety of glassy materials and networks [39]. Setting the exponents a and b both to unity and A to $(2\tilde{E}_Y\tau_r)^{-1}$ would correspond to the Maxwell material analyzed above, whereas for the cytoskeleton $a = 0.5$ and $b = 1$ [40, 41]. If the elastic response is instantaneous compared to viscoelastic relaxation, Eq. (13) determines the cavity growth rate via $dr/dt = rd\varepsilon/dt$, and together with Eq. (7), the ripening of clusters (Fig. 4).

Under viscoelasticity-limited growth, Eq. (8), and small elastic strain, $\lambda \sim 1$, Eq. (13) can be analytically integrated to obtain the general growth equation for viscoelastic ripening,

$$\bar{R}(t) = \gamma \left(\frac{Ab}{a} \right)^{1/b} t^{a/b}, \quad (14)$$

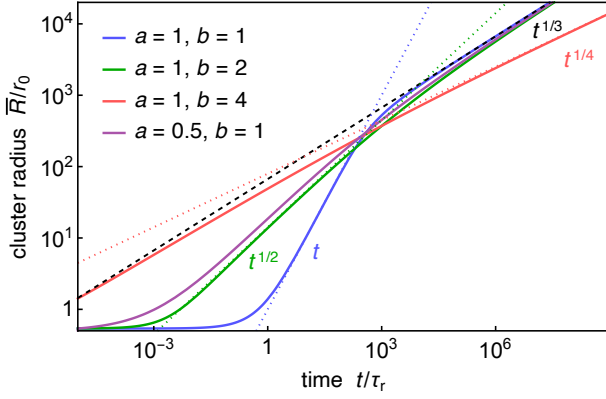


FIG. 4. Ripening behavior at different values of the power-law exponents in the strain rate, Eq. (13). Numerical prediction is obtained by solving Eqs. (7) and (13) (solid lines) with corresponding asymptotic laws for Ostwald [dashed black line, Eq. (5)] and viscoelastic [dotted lines, Eq. (14)] ripening. Prefactors: $Cc_0^{\text{sat}} = 10^5 r_0^3 / (\gamma \tau_r)$, $E_Y \gg \gamma / r_0$ and $A\tau_r^a (\gamma / r_0)^b = 1, 100, 10^7, 3000$, for the blue, green, red and purple lines, respectively.

which agrees with the full numerical solution within the viscoelastic growth regime (Fig. 4). This regime is bounded by the minimum cavity size r_0 and the crossover to the Ostwald ripening regime. The latter is obtained by equating the LSW and viscoelastic growth rates [Eq. (5) and the time derivative of Eq. (14)], yielding the crossover size

$$R_c(t) = r_m \tilde{\tau}^{\frac{1}{3-b}}. \quad (15)$$

Here r_m is the individual particle size, which sets the length scale, and $\tilde{\tau}$ the dimensionless relaxation parameter

$$\tilde{\tau} = \frac{8Dc^{\text{sat}}\gamma^{1-b}t^{1-a}}{27Ac_A^2 k_B T r_m^{3-b}}, \quad (16)$$

that compares the diffusion rate D to the viscoelastic relaxation factor A .

If the initial elastic expansion of cavities λ_c is significant, $\lambda_c \gg 1$, viscoelastic growth is preceded by a purely elasticity-controlled regime bounded by $r_0 < \bar{R} < \lambda_c r_0$, that does not depend on relaxation properties [5]. Figure 5 summarizes the growth regimes [47]. Interestingly, for a strongly shear-thinning material the behavior becomes qualitatively different from a Maxwell material. At $b > 3$ the slope of the boundary in Fig. 5 turns negative; small clusters are limited by Ostwald ripening, while larger domains fall into the viscoelastic ripening regime (Fig. 4).

Having extensively analyzed viscoelastic relaxation, we note that the viscoelastic matrix could form a brittle crack if the elastic stress exceeds the fracture strength $p_{\text{frac}} = \sqrt{E_Y \Gamma / R}$ and $R \geq \Gamma / E_Y$, with Γ the fracture energy of the material [4]. We find the elastic stress that can be produced by surface tension-driven domain

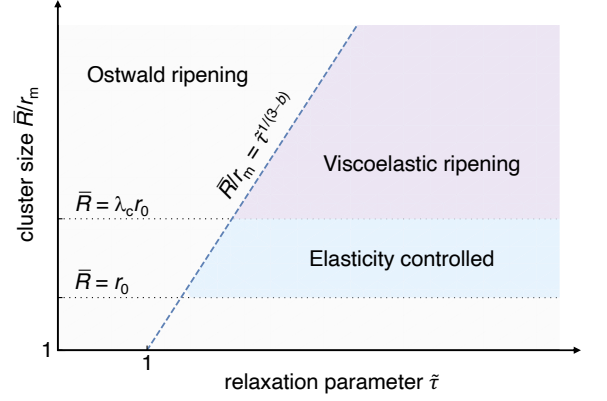


FIG. 5. Theoretical diagram delineating the domain growth regimes in a general viscoelastic material on a double-logarithmic scale: Ostwald (light grey), elasticity controlled (light blue) and viscoelastic ripening (light purple). The boundaries are determined by the initial cavity size r_0 (lower dotted line), the reversible elastic expansion λ_c (upper dotted line) and the crossover to Ostwald ripening (dashed line) as a function of the relaxation parameter $\tilde{\tau}$, Eq. (16). For a Maxwell material ($a = 1$ and $b = 1$) the relaxation parameter becomes proportional to the Maxwell relaxation time, $\tilde{\tau} \propto \tau_r$.

growth is limited to $p_{\text{el}} \sim \gamma / R$, Eq. (8). Thus, formation of a brittle crack would require the surface tension to exceed the fracture energy, $\gamma > \Gamma$. However, since surface tension is typically orders of magnitude smaller than the fracture energy [4], we conclude that viscoelastic relaxation is the dominant out-of-equilibrium process leading to stress relaxation in surface-tension driven coarsening.

V. CONCLUSIONS

We have addressed the problem of phase separation within a viscoelastic material, a question of fundamental importance to different classes of soft materials. Through a combination of analytical calculations and Monte Carlo simulation, we have demonstrated that such systems can exhibit a new type of domain ripening behavior that is distinct from the standard Ostwald ripening process. Our analytical results, supported by MC simulations, show that ripening of phase-separated domains typically exhibits three distinct regimes: (i) elasticity-controlled ripening and arrest on short time scales; (ii) viscoelastic ripening on intermediate time scales with a material-dependent ripening exponent α , e.g., $\alpha \sim 1$ for a Maxwell material; and (iii) Ostwald ripening with $\alpha = 1/3$ in the long time limit. Quantitative experimental verification could be realized by inducing phase separation in a viscoelastic gel with a known constitutive relation and measuring the domain growth over multiple orders of magnitude [cf. Figs. 3 and 4].

Our findings provide insight into phase separation within a wide variety of viscoelastic materials, includ-

ing dense polymer solutions, gels and biological networks like the cytoskeleton. Whereas covalently cross-linked gels or glassy plastics at room temperature exhibit only marginal viscoelastic relaxation, many materials exhibit creep flow and thus domain growth is possible on sufficiently long time scales of years or even centuries [37]. Thus, our findings may have implications for predicting the aging and long-term stability of materials, which are often determined by (micro)phase separation and domain growth, and could explain the coarsening mechanism observed in old oil paintings [20].

Interestingly, our results suggest that cells could regulate the domain size of membrane-less organelles [21] by controlling the viscoelastic properties of the surrounding cytoskeleton network. Conversely, measuring the coarsening exponent could allow determination of the unknown viscoelastic properties of cellular structures [27]. Whereas the present work focuses on passive, surface-tension-driven phase separation, qualitatively different ripening regimes could emerge if condensation and growth are driven by active processes [48]. Our perturbation approach offers an avenue to explore such driven systems.

Lastly, we note that the framework presented can be applied to both fluid and solid spheroidal inclusions, since the stress inside solid spheroidal inclusions is constant [49]. Although crystalline precipitates are often faceted [4], for a compact, convex inclusion the required corrections are expected to be small [28], so that our framework qualitatively applies to crystalline inclusions as well.

VI. METHODS

A. Derivations

1. Nonlinear elasticity

The Gent phenomenological model [30, 31] is valid for extension ratios that are not too large, $\lambda \lesssim 10$, whereas for larger extension ratios additional nonlinear effects due to finite chain extensibility come into play [30, 33]. We model these strain-hardening effects, which prevent an infinite expansion at $p \geq p_c$, by adding an additional power-law term with prefactor E_c ,

$$p_{\text{el}}(\lambda) = \frac{E_Y}{6} (5 - 4\lambda^{-1} - \lambda^{-4}) + E_c E_Y (\lambda - 1)^\gamma. \quad (17)$$

Any positive exponent γ will lead to a divergent pressure in the limit of large expansion ratios, and the value of the exponent determines the sharpness of the pressure–expansion relation. We choose the lowest even exponent, $\gamma = 2$, ensuring that the response is symmetric at $\lambda = 1$ and that above the cavitation pressure the cluster expansion is limited to $\lambda_c \sim E_c^{-1/2}$.

The elastic energy of a spherical cavity is equal to the

reversible pressure work,

$$\begin{aligned} E_{\text{el}}(R, r) &= 4\pi \int_r^R p_{\text{el}}(r'/r) r'^2 dr' \\ &= \frac{4\pi r^3 E_Y}{3} \left[\left(\frac{5}{6} \lambda^3 - \lambda^2 + \frac{1}{2} \lambda^{-1} - \frac{1}{3} \right) \right. \\ &\quad \left. + E_c \left(\frac{3}{5} \lambda^5 - \frac{3}{2} \lambda^4 + \lambda^3 - \frac{1}{10} \right) \right]. \end{aligned} \quad (18)$$

In comparison, the elastic energy of a spherical cavity in an isotropic linearly elastic solid is [28]

$$E_{\text{el, lin}}(\lambda) = \frac{4\pi E_Y}{1 + \nu} r^3 (\lambda - 1)^2. \quad (19)$$

In the limit $\lambda \rightarrow 1$ Eq. (18) reduces to Eq. (19) at Poisson ratio $\nu = 0.5$.

In all calculations we employ the full nonlinear elastic energy, Eq. (18). At $\lambda \sim 1$, where the linear elasticity approximation, Eq. (19), applies, our results are generally valid for any linear elastic material at any ν , provided that the prefactor E_Y is rescaled to $3E_Y/[2(1+\nu)]$. Moreover, we assume that there is no pinning of clusters or droplets to the cavity walls, $p(\lambda) = 0$ for $\lambda < 1$ and, consequently, $E_{\text{el}}(\lambda) = 0$ for $\lambda < 1$.

The equilibrium cluster size can be calculated by starting with the classical nucleation theory (CNT), which assumes that the free energy F_1 of a single spherical cluster of radius R is composed of a surface term and a volume term. To account for elastic deformation energy, we add an elastic term $E_{\text{el}}(R, r)$, yielding the total free energy,

$$F_1 = 4\pi\gamma R^2 + 4\pi R^3 f_v/3 + E_{\text{el}}(R, r), \quad (20)$$

where f_v is the free-energy density of the condensed cluster that is determined by the chemical potential of individual particles that constitute the cluster. Using this expression we can compute the equilibrium cluster size R .

2. Viscoelastic relaxation

Since the pressure depends only on the expansion ratio λ , the elastic energy Eq. (18) is separable into a prefactor proportional to the cavity volume r^3 and a dimensionless energy density term $W(\lambda)$ that depends only on λ ,

$$E_{\text{el}}(r, \lambda) = E_Y r^3 W(\lambda). \quad (21)$$

The elastic energy decreases through increase of the cavity size r ,

$$\left(\frac{\partial E_{\text{el}}}{\partial t} \right)_R = \left(\frac{\partial E_{\text{el}}}{\partial r} \right)_R \left(\frac{\partial r}{\partial t} \right)_R. \quad (22)$$

Using Eqs. (2) and (21) and noting that R and r are independent variables, $\partial r/\partial R = 0$, we find that the cavity growth rate depends only on the logarithmic derivative of $W(\lambda) = E_{\text{el}}/(E_Y r^3)$, Eq. (3). For the extended Gent elastic model Eq. (18) this derivative is

$$\frac{\partial \ln W(\lambda)}{\partial \ln \lambda} = \frac{5\lambda^4/6 - 2\lambda^3/3 - 1/6 + E_c\lambda^4(\lambda - 1)^2}{5\lambda^4/18 - \lambda^3/3 - \lambda/9 + 1/6 + E_c\lambda(\lambda^5/5 - \lambda^4/2 + \lambda^3/3 - 1/30)} . \quad (23)$$

Equations (3) and (23) describe the nonlinear viscoelastic response of a strained spherical cavity. At low strain, $\lambda \rightarrow 1$, we can use the first-order approximation to Eq. (23), obtaining $\frac{\partial \ln W(\lambda)}{\partial \ln \lambda} \approx 2/(\lambda - 1) + 9/2$ and thus recovering the linear Maxwell material relaxation,

$$\frac{dr}{dt} = \frac{R - r}{\tau_r} . \quad (24)$$

B. Monte Carlo simulations

The simulated system comprises $N_p = 25000$ particles suspended in an implicit solvent and placed in a periodic cubic box of linear size $L = 70d_{\text{LJ}}$. The pair interaction between particles of diameter d_{LJ} and center-to-center distance d_{ij} is modeled via a Lennard-Jones (LJ) potential $U_{\text{LJ}}(d_{ij})$ with cut-off $2.5d_{\text{LJ}}$ and interaction strength ϵ_{LJ} . To preserve the appropriate diffusion dynamics of individual particles, we only use local MC moves, consisting of a random displacement of a single particle to a position within a sphere of radius $d_{\text{LJ}}/2$, centered on the original position of the particle. The simulation time scale $\tau = d_{\text{LJ}}^2/40D$ is thus defined by the size of the particles and their diffusion constant D .

This standard LJ system is coupled to a viscoelastic background medium with embedded spherical cavities. Every cluster containing two or more particles is considered to be in phase A and is subject to elastic stress, whereas isolated particles are considered to be in phase B and are not subject to elastic stress. When a dimer (a two-particle cluster) forms, a cavity with initial radius r_0 is created at \mathbf{r}_{cav} , the center of mass of the two particles. This position remains fixed as the cluster grows, unless the cluster fully dissolves into individual particles, at which point the memory of the cavity location disappears. The elastic energy of the cavity is determined by the mismatch between the radii of the cluster R and of the cavity r . Viscoelastic relaxation effects are modeled via dissipative expansion of cavities. The cavity growth rate \dot{r} is obtained from viscoelastic relaxation [Eq. (2)]. Cavities are expanded after each MC cycle of N_p attempted displacement moves via $r \rightarrow r + \tau \dot{r}$.

To calculate the elastic energy we assume a dilute situation in which individual clusters k of particles do not interact through elastic deformations of the surrounding medium and the elastic energy of the system is given by the sum of individual cluster contributions $E_{\text{el},k}$. The total energy of the system is thus

$$E = \sum_{i,j} U_{\text{LJ}}(d_{ij}) + \sum_k E_{\text{el},k} , \quad (25)$$

where the first sum is performed over all pairs of particles and the second sum over all clusters k . To compute the

location and position of the clusters we use a neighbor-based cluster identification algorithm. Two particles are considered neighbors (and thus belong to the same cluster) if their center-to-center distance is less than $1.5d_{\text{LJ}}$. Each cluster is characterized by its center-of-mass position \mathbf{r}_k and radius of gyration $r_{g,k}$ that is calculated from the positions of the individual particles in the cluster,

$$r_{g,k}^2 = r_{\text{gcm},k}^2 + \frac{3}{20} d_{\text{LJ}}^2 , \quad (26)$$

where the first term on the right-hand side is the radius of gyration obtained from the centers of mass of all particles and the second term is the radius of gyration of an individual particle. Since isolated clusters attain a spherical shape with radius $R_k = r_{g,k} \sqrt{5/3}$, the coupling with the elastic medium depends only on $r_{g,k}$ and \mathbf{r}_k . The elastic energy due to cavity expansion $E_{\text{ex},k}$ is obtained by integrating the elastic pressure from the unstressed cavity size r_k to the expanded size R_k , $E_{\text{ex},k} = \int_{r_k}^{R_k} 4\pi(r')^2 p_{\text{el}}(r'/r_k) dr'$ for $R_k > r_k$, and $E_{\text{ex},k} = 0$ otherwise. To represent the displacement $d_k = |\mathbf{r}_k - \mathbf{r}_{\text{cav},k}|$ of the center of mass \mathbf{r}_k of the cluster with respect to the cavity position $\mathbf{r}_{\text{cav},k}$, we add a linear elastic displacement term $E_{\text{d},k} = \pi E_Y R_k d_k^2$ for $R_k > r_k + d_k$ and $E_{\text{d},k} = 0$ otherwise [28]. The total elastic energy of a specific cluster is $E_{\text{el},k} = E_{\text{ex},k} + E_{\text{d},k}$, which both suppresses the growth and immobilizes the clusters. No pinning of clusters to cavity walls is considered, i.e., partially filled cavities are allowed and do not provide additional free-energy contributions.

Since the aim is not to study coalescence but surface-tension-driven ripening of spherical clusters, we restrict MC moves to single-particle moves that do not lead to coalescence or breaking of existing clusters. Such coalescence events can occur in principle but are very rare and negligible at dilute conditions. Accurately incorporating coalescence would be difficult within our simulation setup, because at the point of coalescence the cluster shape is highly nonspherical and thus the elastic deformation of the surrounding medium is challenging to calculate. Therefore, we exclude the influence of possible coalescence events, by rejecting any MC move that involves the merging of two existing clusters or the breaking of a cluster into two disjoint parts where at least one of these parts is not a free, unbound particle. Our simulations thus always model surface-tension-driven ripening of isolated spherical clusters in the dilute limit where individual clusters do not interact directly.

Phase equilibrium is determined by the LJ interaction parameter ϵ_{LJ} and the density $\rho = N_p/L^3$, while the viscoelastic properties are determined by the modulus E_Y , the coefficient E_c and the viscoelastic relaxation time relative to the diffusion time scale τ_r/τ . The calcu-

lations are performed at temperature $T = \epsilon_{\text{LJ}}/(1.8k_{\text{B}})$, which is in a two-phase coexistence region of the LJ phase diagram (cf. Fig. 2a,b). We set $E_{\text{Y}} = k_{\text{B}}T/d_{\text{LJ}}^3$ and $r_0 = d_{\text{LJ}}$, with r_0 the initial cavity size corresponding to a flexible gel with crosslink distance r_0 [29]. This choice permits simulations of sufficiently large systems (i.e., containing multiple coarsening droplets) over sufficiently long time scales, thus making it possible to calculate the growth exponents (cf. Fig. 2). Using $r_0 \gg d_{\text{LJ}}$ would more accurately capture experimental systems, but would be prohibitively expensive to simulate. We anticipate that any choice satisfying $r_0 \geq d_{\text{LJ}}$ yields the same predictions, since the molecular details on length scales smaller than the mesh size should not affect the condensation and coarsening process in the viscoelastic regime. By choosing $r_0 = d_{\text{LJ}}$ we miss details of the process on length scales smaller than the mesh size, where viscoelastic effects are not relevant.

The average cluster size n and radius \bar{R} are calculated from all clusters with more than five particles, to avoid counting transient small aggregates. The mapping between simulation and theoretical parameters is obtained from equilibrium properties of the LJ fluid and the simulation time scale τ . We set $\gamma = 3.06k_{\text{B}}Td_{\text{LJ}}^{-2}$ and $c_{\text{A}} = 1.14d_{\text{LJ}}^{-3}$, which are found by extrapolating LJ fluid parameters [50] to $\epsilon_{\text{LJ}} = 1.8k_{\text{B}}T$, while $c_0^{\text{sat}} = 4.3 \cdot 10^{-4}d_{\text{LJ}}^{-3}$ is obtained directly from MC simulations.

C. Perturbation theory

We consider viscoelastic effects in a first-order perturbative expansion of the LSW Ostwald ripening theory, Eq. (5). For clarity we use dot notation for derivatives, $\dot{R} \equiv dR/dt$. The growth rate of the mean cluster size $\dot{\bar{R}}$ depends on the thermodynamic driving force f , the derivative of the free-energy density of N spherical clusters at constant total volume $V = \frac{4}{3}\pi N\bar{R}^3$,

$$f = -\left.\frac{\partial(F/V)}{\partial\bar{R}}\right|_V. \quad (27)$$

The growth rate can also depend on the kinetic prefactors, such as the diffusion constant, which determine monomer transport. Here we assume that monomers can diffuse uninhibited through the viscoelastic medium, so that the kinetic prefactors are constant. Thus, the first-order correction to LSW ripening due to viscoelastic effects is

$$\dot{\bar{R}} = \dot{\bar{R}}_0 + \left.\frac{\partial\dot{\bar{R}}}{\partial f}\right|_{f_0} (f - f_0), \quad (28)$$

where $\dot{\bar{R}}_0$ and f_0 are the growth rate and the driving force, respectively, in the reference (LSW) system. Within this first-order expansion the relative cluster size distribution $h(R/\bar{R})$ is time-independent and given by

the LSW theory [1]. We assume that the expansion ratio λ has the same value for all clusters in $h(R/\bar{R})$, so that the joint distribution of clusters and cavities is

$$\psi(R/\bar{R}, r/\bar{r}) = h(R/\bar{R})\delta(R - \lambda r), \quad (29)$$

with λ the sole variable and $\delta(x)$ the Dirac delta function.

To calculate the first-order correction we need to evaluate the total free energy F . The free energy of a single cluster F_1 is determined by the surface tension and elastic energy contributions [cf. Eq. (20)] and the total free energy is obtained by summing over all clusters in the system, $F = \sum_i F_{1,i}(R_i, r_i)$. Using the mean-field approximation $F = NC_\psi F_1(\bar{R}, \bar{r})$ in Eq. (27), where $F_1(\bar{R}, \bar{r})$ is the free energy of an average-sized cluster, we find the reference driving force $f_0 = 3C_\psi\gamma/(C'_\psi\bar{R}^2)$ and the viscoelastic contribution $f - f_0 = 3C_\psi/(4\pi C'_\psi)\partial(E_{\text{el}}/\bar{R}^3)/\partial\bar{R}$. The size distribution (ψ) dependent prefactors $C_\psi = \bar{F}_1(R, r)/F_1(\bar{R}, \bar{r})$ and $C'_\psi = \bar{R}^3/\bar{r}^3$ are assumed time-independent. Using these expressions in Eq. (28) we obtain the first-order perturbative correction to the LSW theory [Eq. (7)].

The assumption of a time-independent distribution does not apply in the case of elastic arrest, where $h(R/\bar{R})$ would gradually change to a uniform size distribution [51]. Capturing the time dependence in $h(R/\bar{R})$ would require a second-order expansion, for which we did not find an analytically tractable expression. However, we do not expect second-order effects to qualitatively affect the growth rate. Even in the case of elastic arrest, the first-order theory, Eq. (7), already correctly predicts an exponential approach of \bar{R} to an equilibrium value [15].

To obtain an analytical relation between stress and cluster size at small deformations ($\lambda \sim 1$) we consider a closed system containing a total constant volume V of the condensed phase. Assuming that clusters can freely exchange material via exchange of individual particles, the equilibrium number of clusters N is determined by the minimization of the total free energy of the system, $F = NC_\psi F_1(R, r)$ [cf. Eq. (20)]. Thus, the equilibrium values for N and R are obtained by setting

$$\left(\frac{\partial(NC_\psi F_1)}{\partial R}\right)_V = 0. \quad (30)$$

Solving this equation in the limit $N \rightarrow \infty$ yields

$$4\pi R^2\gamma = R\frac{\partial E_{\text{el}}}{\partial R} - 3E_{\text{el}}. \quad (31)$$

The elastic energy can generally be expressed as a polynomial expansion, $E_{\text{el}} = A\varepsilon^2 + B\varepsilon^3 + C\varepsilon^4 + \dots$, around its zero value, $E_{\text{el}}(\varepsilon = 0) = 0$, with the strain $\varepsilon = R/r - 1$. Thus, the energy scales with its derivative as $E_{\text{el}} \sim \varepsilon r \frac{\partial E_{\text{el}}}{\partial R}$, so that under small deformations, $\varepsilon \rightarrow 0$, the last term in Eq. (31) can be neglected. Expressing the first term on the right-hand side of Eq. (31) in terms of the radial elastic stress, $\sigma = \frac{\partial E_{\text{el}}}{\partial R} \frac{1}{4\pi R^2}$, we observe that

this stress is determined solely by the surface tension and the cluster radius,

$$\sigma = \gamma/R. \quad (32)$$

Interestingly, σ does not depend on the elastic properties of the material or on the cavity size r .

ACKNOWLEDGMENTS

We thank Peter Voorhees and Robert Style for enlightening discussions. This work was supported by the E.U.

Horizon 2020 program under the Marie Skłodowska-Curie fellowship No. 845032, the U.S. Department of Energy, Office of Science, Office of Basic Energy Sciences, Division of Materials Sciences and Engineering, under Award Number DE-SC0020885, and the Center for Scientific Studies in the Arts at Northwestern University, which is funded by the Andrew W. Mellon Foundation.

-
- [1] L. Ratke and P. W. Voorhees, Nucleation, growth and coarsening, in *Growth and Coarsening: Ostwald Ripening in Material Processing* (Springer, Berlin, 2002) pp. 205–224.
 - [2] F. R. N. Nabarro, The strains produced by precipitation in alloys, *Proc. R. Soc. London, Ser. A* **175**, 519 (1940).
 - [3] R. W. Style, T. Sai, N. Fanelli, M. Ijavi, K. Smith-Mannschott, Q. Xu, L. A. Wilen, and E. R. Dufresne, Liquid-liquid phase separation in an elastic network, *Phys. Rev. X* **8**, 011028 (2018).
 - [4] J. Y. Kim, Z. Liu, B. M. Weon, T. Cohen, C.-Y. Hui, E. R. Dufresne, and R. W. Style, Extreme cavity expansion in soft solids: Damage without fracture, *Sci. Adv.* **6** (2020).
 - [5] K. A. Rosowski, T. Sai, E. Vidal-Henriquez, D. Zwicker, R. W. Style, and E. R. Dufresne, Elastic ripening and inhibition of liquid-liquid phase separation, *Nature Phys.* **16**, 422 (2020).
 - [6] M. Kothari and T. Cohen, Effect of elasticity on phase separation in heterogeneous systems, *Journal of the Mechanics and Physics of Solids* **145**, 104153 (2020).
 - [7] E. Vidal-Henriquez and D. Zwicker, Theory of droplet ripening in stiffness gradients, *Soft Matt.* **16**, 5898 (2020).
 - [8] X. Wei, J. Zhou, Y. Wang, and F. Meng, Modeling elastically mediated liquid-liquid phase separation, *Phys. Rev. Lett.* **125**, 268001 (2020).
 - [9] E. Vidal-Henriquez and D. Zwicker, Cavitation controls droplet sizes in elastic media, *Proceedings of the National Academy of Sciences* **118**, e2102014118 (2021).
 - [10] P. Ronceray, S. Mao, A. Košmrlj, and M. P. Haataja, Liquid demixing in elastic networks: Cavitation, permeation, or size selection?, *Europhys. Lett.* **137**, 67001 (2022).
 - [11] E. D. Siggia, Late stages of spinodal decomposition in binary mixtures, *Phys. Rev. A* **20**, 595 (1979).
 - [12] H. Tanaka, Viscoelastic phase separation, *J. Phys.: Condens. Matter* **12**, R207 (2000).
 - [13] H. Tabuteau, S. Mora, G. Porte, M. Abkarian, and C. Ligoure, Microscopic mechanisms of the brittleness of viscoelastic fluids, *Phys. Rev. Lett.* **102**, 155501 (2009).
 - [14] R. Pascova, I. Gutzow, and J. Schmelzer, A model investigation of the process of phase formation in photochromic glasses, *J. Mater. Sci.* **25**, 921 (1990).
 - [15] J. Schmelzer, I. Gutzow, and R. Pascova, Kinetics of phase segregation in elastic and viscoelastic media, *J. Cryst. Growth* **104**, 505 (1990).
 - [16] J. Schmelzer, R. Pascova, and I. Gutzow, Cluster growth and ostwald ripening in viscoelastic media, *Phys. Stat. Sol. (a)* **117**, 363 (1990).
 - [17] J. W. P. Schmelzer, R. Müller, J. Möller, and I. S. Gutzow, Theory of nucleation in viscoelastic media: application to phase formation in glassforming melts, *J. Non-Cryst. Solids* **315**, 144 (2003).
 - [18] H. Tanaka, T. Araki, T. Koyama, and Y. Nishikawa, Universality of viscoelastic phase separation in soft matter, *J. Phys.: Condens. Matter* **17**, S3195 (2005).
 - [19] M. Tateno and H. Tanaka, Power-law coarsening in network-forming phase separation governed by mechanical relaxation, *Nature Communications* **12**, 912 (2021).
 - [20] F. Casadio, K. Keune, P. Noble, A. van Loon, E. Hendriks, S. A. Centeno, and G. Osmond, eds., *Metal Soaps in Art: Conservation and Research* (Springer, 2019).
 - [21] M. Feric, N. Vaidya, T. S. Harmon, D. M. Mitrea, L. Zhu, T. M. Richardson, R. W. Kriwacki, R. V. Pappu, and C. P. Brangwynne, Coexisting liquid phases underlie nucleolar subcompartments, *Cell* **165**, 1686 (2016).
 - [22] S. Alberti, A. Gladfelter, and T. Mittag, Considerations and challenges in studying liquid-liquid phase separation and biomolecular condensates, *Cell* **176**, 419 (2019).
 - [23] S. C. Weber, Sequence-encoded material properties dictate the structure and function of nuclear bodies, *Curr. Opin. Cell Biol.* **46**, 62 (2017).
 - [24] L. Jawerth, E. Fischer-Friedrich, S. Saha, J. Wang, T. Franzmann, X. Zhang, J. Sachweh, M. Ruer, M. Ijavi, S. Saha, J. Mahamid, A. A. Hyman, and F. Jülicher, Protein condensates as aging Maxwell fluids, *Science* **370**, 1317 (2020).
 - [25] D. Michieletto and M. Marendza, Rheology and viscoelasticity of proteins and nucleic acids condensates, *JACS Au* **2**, 1506 (2022).
 - [26] Y. Shin, Y.-C. Chang, D. S. W. Lee, J. Berry, D. W. Sanders, P. Ronceray, N. S. Wingreen, M. Haataja, and C. P. Brangwynne, Liquid nuclear condensates mechanically sense and restructure the genome, *Cell* **175**, 1481 (2018).
 - [27] D. S. W. Lee, N. S. Wingreen, and C. P. Brangwynne, Chromatin mechanics dictates subdiffusion and coarsening dynamics of embedded condensates, *Nature Phys.* **17**, 531 (2021).
 - [28] L. D. Landau and E. M. Lifshitz, *Theory of Elasticity*,

- Course of Theoretical Physics, Vol. 3 (Pergamon, London, 1959).
- [29] M. Rubinstein and R. H. Colby, *Polymer Physics* (Oxford University Press, Oxford, 2003).
 - [30] A. N. Gent and C. Wang, Fracture mechanics and cavitation in rubber-like solids, *J. Mater. Sci.* **26**, 3392 (1991).
 - [31] A. N. Gent, A new constitutive relation for rubber, *Rubber Chem. Technol.* **69**, 59 (1996).
 - [32] J. A. Zimmerlin, N. Sanabria-DeLong, G. N. Tew, and A. J. Crosby, Cavitation rheology for soft materials, *Soft Matt.* **3**, 763 (2007).
 - [33] S. B. Hutchens, S. Fakhouri, and A. J. Crosby, Elastic cavitation and fracture *via* injection, *Soft Matt.* **12**, 2557 (2016).
 - [34] The exact expression for $p_{\text{el}}^{\text{lim}}$ is not of crucial importance. Any functional form that limits the expansion ratio, $p_{\text{el}}^{\text{lim}} \sim \lambda^\kappa$ as $\lambda \rightarrow \infty$, with $\kappa > 0$, could be used.
 - [35] W. Denissen, M. Droesbeke, R. Nicolaÿ, L. Leibler, J. M. Winne, and F. E. Du Prez, Chemical control of the viscoelastic properties of vinylogous urethane vitrimers, *Nature Comm.* **8**, 14857 (2017).
 - [36] B. M. El-Zaatari, J. S. A. Ishibashi, and J. A. Kalow, Cross-linker control of vitrimer flow, *Polym. Chem.* **11**, 5339 (2020).
 - [37] G. Capiel, E. Hernández, N. E. Marcovich, and M. A. Mosiewicki, Stress relaxation behavior of weldable crosslinked polymers based on methacrylated oleic and lauric acids, *Eur. Polym. J.* **132**, 109740 (2020).
 - [38] Y. Mulla, F. C. MacKintosh, and G. H. Koenderink, Origin of slow stress relaxation in the cytoskeleton, *Phys. Rev. Lett.* **122**, 218102 (2019).
 - [39] P. Sollich, F. Lequeux, P. Hébraud, and M. E. Cates, Rheology of soft glassy materials, *Phys. Rev. Lett.* **78**, 2020 (1997).
 - [40] C. P. Broedersz, M. Depken, N. Y. Yao, M. R. Pollak, D. A. Weitz, and F. C. MacKintosh, Cross-link-governed dynamics of biopolymer networks, *Phys. Rev. Lett.* **105**, 238101 (2010).
 - [41] N. Desprat, A. Richert, J. Simeon, and A. Asnacios, Creep function of a single living cell, *Biophys. J.* **88**, 2224 (2005).
 - [42] R. B. Bird, R. C. Armstrong, O. Hassager, and C. F. Curtiss, Differential constitutive equations, in *Dynamics of polymer liquids* (Wiley, New York, 1987) pp. 341–423.
 - [43] A. Baldan, Progress in Ostwald ripening theories and their applications to nickel-base superalloys. Part I: Ostwald ripening theories, *J. Mater. Sci.* **7**, 2171 (2002).
 - [44] C. Jeppesen and O. G. Mouritsen, Universality of ordering dynamics in conserved multicomponent systems, *Phys. Rev. B* **47**, 14724 (1993).
 - [45] I. M. Lifshitz and V. V. Slyozov, The kinetics of precipitation from supersaturated solid solutions, *J. Phys. Chem. Solids* **19**, 35 (1961).
 - [46] Viscoelastic ripening could potentially be found in a one-component system provided $c_A \ll r_m^{-3}$, which would occur if gas bubbles nucleate within a dense phase and grow via surface-tension-driven coarsening.
 - [47] This figure does not cover the case in which initial nucleation and growth of small clusters follows a $R \sim t^2$ scaling [1].
 - [48] D. Zwicker, R. Seyboldt, C. A. Weber, A. A. Hyman, and F. Jülicher, Growth and division of active droplets provides a model for protocells, *Nature Phys.* **13**, 408 (2017).
 - [49] J. D. Eshelby, The determination of the elastic field of an ellipsoidal inclusion, and related problems, *Proc. R. Soc. London, Ser. A* **241**, 376 (1957).
 - [50] J. Janeček, Long range corrections in inhomogeneous simulations, *J. Phys. Chem. B* **110**, 6264 (2006).
 - [51] J. Schmelzer and J. Möller, Evolution of the cluster size-distribution function for Ostwald ripening in viscoelastic media, *Phase Transitions* **38**, 261 (1992).

SI: Phase separation and ripening in a viscoelastic gel

Tine Curk^{1,*} and Erik Luijten^{1,2,†}

¹*Department of Materials Science & Engineering,
Northwestern University, Evanston, Illinois 60208, USA*

²*Departments of Engineering Sciences & Applied Mathematics, Chemistry,
and Physics & Astronomy, Northwestern University, Evanston, Illinois 60208, USA*

(Dated: March 23, 2023)

I. UPPER-CONVECTED MAXWELL MODEL IN A SPHERICALLY SYMMETRIC GEOMETRY

We consider a droplet in a viscoelastic medium described by the Upper-convected Maxwell model. The constitutive relation of the upper-convected Maxwell model [1] is

$$\mathbf{T} + \lambda_1 \mathbf{T}_{(1)} = -\eta_0 \dot{\boldsymbol{\gamma}} \quad (\text{S1})$$

where \mathbf{T} is the stress tensor and $\boldsymbol{\gamma}$ the strain tensor, $\lambda_1 = \eta_0/G$ the relaxation time with η_0 the zero-shear-rate viscosity and G the shear modulus. $\mathbf{T}_{(1)}$ is the upper-convected time derivative of the stress tensor

$$\mathbf{T}_{(1)} = \frac{\partial}{\partial t} \mathbf{T} + \mathbf{v} \cdot \nabla \mathbf{T} - (\nabla \mathbf{v})^\dagger \cdot \mathbf{T} - \mathbf{T} \cdot \nabla \mathbf{v} \quad (\text{S2})$$

with \mathbf{v} the velocity of the medium, $\nabla \mathbf{v}$ the gradient of \mathbf{v} and superscript \dagger denotes the transpose of a tensor. The rate of strain tensor is

$$\dot{\boldsymbol{\gamma}} = (\nabla \mathbf{v})^\dagger + \nabla \mathbf{v}. \quad (\text{S3})$$

For an isolated spherical droplet the problem is spherically symmetric. The velocity is radially symmetric, $v_\theta = v_\phi = 0$ and $\partial v_r / \partial \theta = \partial v_r / \partial \phi = 0$. The velocity gradient in spherical coordinates is

$$\nabla \mathbf{v} = \begin{pmatrix} \frac{\partial v_r}{\partial r} & 0 & 0 \\ 0 & \frac{v_r}{r} & 0 \\ 0 & 0 & \frac{v_r}{r} \end{pmatrix}. \quad (\text{S4})$$

Due to the absence of rotational deformations both the stress and strain tensors are diagonal. The convective derivative is also diagonal

$$\mathbf{v} \cdot \nabla \mathbf{T} = \begin{pmatrix} v_r \frac{\partial T_{rr}}{\partial r} & 0 & 0 \\ 0 & v_r \frac{\partial T_{\theta\theta}}{\partial r} & 0 \\ 0 & 0 & v_r \frac{\partial T_{\phi\phi}}{\partial r} \end{pmatrix}. \quad (\text{S5})$$

Thus, the constitutive relation simplifies to only two independent equations,

$$\frac{T_{rr}}{\lambda_1} + \frac{\partial T_{rr}}{\partial t} + v_r \frac{\partial T_{rr}}{\partial r} = 2 \frac{\partial v_r}{\partial r} (-G + T_{rr}) \quad (\text{S6})$$

and

$$\frac{T_{\theta\theta}}{\lambda_1} + \frac{\partial T_{\theta\theta}}{\partial t} + v_r \frac{\partial T_{\theta\theta}}{\partial r} = 2 \frac{v_r}{r} (-G + T_{\theta\theta}), \quad (\text{S7})$$

while the relation for $\phi\phi$ components is identical to the $\theta\theta$ components [(S7)].

* curk@northwestern.edu

† luijten@northwestern.edu

S2

A. small stress limit

For small stresses $T_{rr}/G \ll 1$, the last term on the right hand side of (S6) can be neglected. Furthermore, at small stresses the velocity v_r also vanishes, $v_r \rightarrow 0$ as $T_{rr} \rightarrow 0$, thus, the last term on the left hand side can also be neglected. Since $T_{rr} \sim T_{\theta\theta}$ the same approximation applies to (S7) and the constitutive relation reduces to

$$\frac{T_{rr}}{\lambda_1} + \frac{\partial T_{rr}}{\partial t} = -2G \frac{\partial v_r}{\partial r} \quad (\text{S8})$$

and

$$\frac{T_{\theta\theta}}{\lambda_1} + \frac{\partial T_{\theta\theta}}{\partial t} = -2G \frac{v_r}{r}. \quad (\text{S9})$$

These two equations are a spherically symmetric case of the Maxwell model given by

$$\mathbf{T} + \lambda_1 \frac{\partial}{\partial t} \mathbf{T} = -\eta_0 \dot{\boldsymbol{\gamma}}. \quad (\text{S10})$$

Therefore, in the small stress limit, the upper-convected Maxwell model reduces to the Maxwell model. While we have focused on the spherically symmetric case, other geometries and approximations to upper-convected derivative are discussed in Ref. [1].

B. model generalizations

The upper-convected Maxwell model considers elasticity and relaxation due to the material viscosity of the polymers. To include effects of the solvent viscosity we need the Oldroyd B-model,

$$\mathbf{T} + \lambda_1 \mathbf{T}_{(1)} = -\eta_0 (\dot{\boldsymbol{\gamma}} + \lambda_2 \boldsymbol{\gamma}_{(2)}), \quad (\text{S11})$$

where $\boldsymbol{\gamma}_{(2)}$ is the second rate-of-strain tensor and λ_2 the retardation time that is determined by the solvent viscosity [1]. For the case of coarsening droplets, the observation of viscoelastic ripening requires the relaxation time λ_1 to be at least a few orders of magnitude larger than the retardation time $\lambda_2/\lambda_1 \sim 0$. In this case the Oldroyd B-model reduces to the upper-convected Maxwell model [(S1)].

Viscoelastic ripening exponent is determined in the small stress limit where all non-linear generalizations of the Oldroyd B-model, such as Giesekus model, the White-Metzner model or the Oldroyd 8-constant model, reduce to the Maxwell model. Thus, we expect the viscoelastic ripening exponent as calculated using the Maxwell model is general to any constitutive relation that reduces to the Maxwell model in the small stress-limit.

[1] R. B. Bird, R. C. Armstrong, O. Hassager, and C. F. Curtiss, Differential constitutive equations, in *Dynamics of polymer liquids* (Wiley, New York, 1987) pp. 341–423.